Exploring the Potential of Co₃O₄@MnO₂@ZnO Enhanced with *Vitex Doniana* Leaf Extract for Supercapacitor Electrode Applications

Raphael Mmaduka Obodo^{1,2,3,4}

https://orcid.org/0000-0001-7418-8526 raphael.obodo@unn.edu.ng raphael.obodo@uaes.edu.ng

Sabastine C. Ezike⁵

https://orcid.org/0000-0003-3962-1624

Sabastine E. Ugwuanyi²

https://orcid.org/0009-0000-6680-5707

Miletus O. Duru⁷

https://orcid.org/0009-0003-0708-2379

Abdoulaye Diallo9

https://orcid.org/0000-0002-4032-0477

Hope Ebere Nsude²

https://orcid.org/0009-0000-5082-6378

Joseph N. Anosike,6

https://orcid.org/0009-0007-6899-4768

Chimezie U. Eze^{2,7}

https://orcid.org/0000-0002-1009-2741

Ugochukwu C. Elejere^{2,8}

https://orcid.org/0000-0001-6426-1865

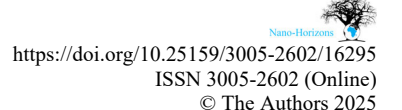
Ishaq Ahmad^{3,4}

https://orcid.org/0000-0002-6573-0392

⁹ Department of Physics and Chemistry, Faculty of Sciences and Technologies of Formation and Education, Cheikh Anta Diop University, Senegal.



Volume 4 | 2025 | #16295 | 26 pages





¹ Department of Physics, University of Agriculture and Environmental Sciences, Nigeria.

² Department of Physics and Astronomy, University of Nigeria.

³ National Centre for Physics, Quaid-i-Azam University, Pakistan.

⁴ NPU-NCP Joint International Research Centre on Advanced Nanomaterials and Defects Engineering, Northwestern Polytechnical University, China.

⁵ Department of Physics, Modibbo Adama University of Technology, Nigeria.

⁶ Department of Industrial Chemistry, University of Nigeria.

⁷ Department of Physics, Federal University of Technology, Nigeria.

⁸ Department of Physics, Federal College of Education, Nigeria.

Abstract

The use of transition metal oxides as supercapacitor electrodes has attracted a great deal of attention because of their properties such as superior electrochemical performances, availability, low toxicity and affordability. It has been noted that Co₃O₄@MnO₂@ZnO composites augmented with *Vitex doniana* leaf extract as an electrode material is being investigated for the first time in the context of supercapacitors. The Co₃O₄@MnO₂@ZnO composite electrode mediated with *Vitex doniana* leaf extract used in this study was produced using the chemical bath deposition technique. The findings demonstrated that Co₃O₄@MnO₂@ZnO nanocomposites enhanced with *Vitex doniana* leaf extract are good material for supercapacitor electrode fabrication. This is demonstrated by the achievement of maximum specific capacitances of 1 215 F/g using cyclic voltammetry and 1 250 F/g at a current density of 0.5 A/g using galvanostatic charge—discharge. After 10 000 complete cycles, Co₃O₄@MnO₂@ZnO (CMZ/150) showed exceptional stability, with a 97.25% retention rate.

Keywords: Electrodes, leaf extract, specific capacitance and efficiency, supercapacitor, *Vitex doniana*.

1 Introduction

Growing public concern over environmental problems brought on by unsuitable industrial practices and unsustainable fossil fuel consumption has been observed in recent years [1], [2]. Finding new forms of green, renewable and non-toxic energy sources is one of the most pressing issues as the energy crisis deepens. Because of supercapacitors' exceptional electrical qualities, which include rapid charging times, extended cycling lives, high reliability and increased power and energy densities, prompted its suggestion as a solution to this problem [3], [4]. In supercapacitor materials, separators, electrodes and electrolytic solutions can influence the working principles of supercapacitors, with the electrode material typically having the greatest impact [5], [6]. Electrochemical properties of electrode materials are greatly influenced by their specific superficial areas, shape, pore size distributions and electrical conductivities; however, producing electrode materials with superior capacitance performances remains a difficult challenge [7], [8].

Researchers are quickly favouring transition metal oxide electrode materials over carbon derivatives and conducting polymer electrode materials owing to their quick redox kinetics and virtuous reversibility, capability to attain huge capacitance and optimum firmness [9]–[11]. The optimal specific capacitance values of composite transition metal oxides or hydroxides are extremely high, reaching up to 2 573 F/g [12], 2 082 F/g [13], 3 560 F/g [14] and 3 500 F/g [15]. However, in practical applications, their real capacitance significance is substantially less than that in perfect standards. This may be caused by their weak redox reversibility, electrical conductivity and

crystallinity, therefore the need for enhancement and strengthening. According to recent studies, nanocomposites typically outperform single components in catalysis [16] [17], biochemical sensing [18], lithium-ion batteries [5] and gas sensing [19] because of their synergistic effects. Higher electrochemical performances are frequently observed in transition metal oxides and hydroxides made up of two or three transition metal components [20]–[22].

With regard to joining three diverse metallic oxides, Obodo et al. [23] assessed 8.0 MeV carbon (C2+) irradiation effects on hydrothermally produced Co3O4-CuO-ZnO@GO electrode aimed at uses of supercapacitors. The authors reported specific capacitance measured by galvanostatic charge-discharge (GCD) at 1 950 and 2 045 F/g at 0.5 A/g and 1.0 A/g current densities and irradiation dosage of 5.0×10^{15} ions/cm². Juma et al. [24] stated that three phases were found in the CuO-NiO-ZnO mixed metal oxides nanocomposite, which indicated the existence of CuO/NiO/ZnO binary heterojunctions. These heterojunctions prompted a significant impact on nanocomposites inclusive performances, and employing metal acetate precursors and monoethanolamine or isopropanol solutions. Habibi and Karimi [25] produced CuO-ZnO-Cu₂O nanocomposites and investigated them. According to their findings, optoelectronics and electronics could benefit from the application of these semiconducting composite oxides. However, Obodo et al. [26] optimised graphitised Co₃O₄@CuO@NiO composites electrode for use in supercapacitors. They reported specific capacitances of 1 258 F/g using a GCD study employing 1.0 A/g current density and 1 312 F/g in cyclic voltammetry (CV) investigation engaging 10.0 mV/s scan rate. After 10 000 cycles, the cycling firmness of various electrodes dried at 100 °C stood at 92.5%, suggesting that annealing at this temperature enhanced the properties of the electrodes.

Vitex doniana is a medium-sized deciduous tree with a rounded, hefty crown and a visible bole that can reach a height of 5 metres [27] [28]. The bark is rough with thin vertical fissures and is pale brown or greyish-white. These trees have oblong scales on their bases [27], [29]. They have opposite, glabrous, 14–34 cm long leaves that typically have five leaflets on 6–14 cm long stalks. The leaves are stalked, whole, ovate, obovate-elliptic or oblong, and measure 8–22 cm in length and 2–9 cm in width. The leaf bases are cuneate and the leaf tips are rounded or emarginated [27]. Vitex doniana leaves comprise various biomolecules that execute reducing and sedative agents in the development of metallic oxide nanoparticles [30]. The biologically active phytochemicals found in Vitex doniana are responsible for shielding the plant from environmental dangers such as pollution, stress, scarcity, UV exposure and pathogenic invasions [30], [31]. They also play a beneficial role in the efficient interactions between metallic ions in composite materials.

Numerous phytochemicals, including alkaloids, flavonoids, proteins, phenols, steroids, glycosides, carbohydrates, terpenoids, tannins, essentials minerals and vitamins, are present in plants [30], [31]. In addition, they have long been used in Africa to cure a wide range of illnesses, including arthrosclerosis, diabetes, cancer, cardiovascular

diseases and neurological disorders [31]. The characteristics and reaction mechanism of bioactive substances such as terpenoids and flavonoids may be integrated into energy-storing equipment that resemble supercapacitors, since their features have been shown in medical applications.

This study fabricated, for the first time, Co₃O₄@MnO₂@ZnO composites enriched with *Vitex doniana* leaf extract for use as supercapacitor electrodes. To increase the electrodes' superficial areas, rate competency, reactions kinetics, satisfactory electroactive points, numerous ions transference paths, conductivity, higher charges assemblage capability and speedy redox reactions kinetics, as well as their electrochemical stability and increased redox capability, *Vitex doniana* leaf extract was used in this study.

2 Materials and Methods

The chemicals used in this experiment were purchased and are of analytical quality from the Sigma-Aldrich store without the need for additional purification. Cobalt sulphate hexahydrate (CoSO₄.6H₂O) (Sigma-Aldrich, 98.7%), manganese (II) sulphate (MnSO₄·H₂O) (Sigma-Aldrich, 98.4%) and zinc sulphate heptahydrate (ZnSO₄·7H₂O)) (Sigma-Aldrich, 99.2%) were employed to provide Co⁺, Mn⁺ and Zn⁺ ions correspondingly. *Vitex doniana* leaf extracts were used in place of the reducing facilitator. Purified water (H₂O) was employed for the dissolving of salts, cleaning of leaves, rinsing, cleaning of flasks, etc. Sodium sulphate (Na₂SO₄) was used for the development of electrolyte engaged throughout electrochemical analysis. Fluorine-doped tin oxide (FTO) glass was employed during the fabrication of these electrodes.

2.1 Producing Vitex Doniana Leaf Extract

Vitex doniana leaves that were good and undamaged were gathered from the Nkwo Lejja Market in Nsukka, Enugu State, Nigeria. After washing the healthy leaves in double-distilled water, they were dried in a room to get rid of the moisture. A blender was used to grind 200 g of these leaves into a fine powder. The powder was transferred to a 500 ml beaker, heated and stirred for 2 hours at 50 °C. The mixture's colour turned dark green after two hours, which revealed the leaf extract. After the extract had cooled to room temperature, it was twice filtered using filter paper (Whatman No. 1) to remove solid impurities. Later, the extract was chilled and stored in a refrigerator at 4 °C and used within 1 week.

2.2 Fabricating Electrode/Nanoparticle

50 ml each of 0.1 M concentrations of various salt precursors of CoSO₄.6H₂O, MnSO₄·H₂O and NiSO₄(H₂O) were prepared, stirred to homogeneity and mixed together. The entire mixed solution was transferred to a 500 ml beaker; the beaker was moved to a magnetic stirrer and heater as shown in Fig. 1. Then, 50 ml of prepared *Vitex doniana* extract was added dropwise using a burette in the continuous stirring and heating at a temperature of 70 °C for 2 hours as shown in Fig. 1. Substrate and

thermometer holders were used to position a well-cleaned and treated rectangle conducting FTO glass that measured 4.0 cm × 4.0 cm, pH meter and thermometer, respectively. A well-cleaned pH meter was also inserted as shown in Fig. 1. At this point, the heater was set at 70 °C and while stirring the leaf extract was added dropwise within 1 hour. The stirring and heating were extended for another 1 hour for homogeneity. The pH of the bath was measured at the expiration of the process. After 2 hours, the beaker was detached and permitted to cool to room temperature. The fabricated electrodes were removed, rinsed with refined water and dehydrated in the oven for 2 hours at 50 °C. Whatman No. 1 filter paper was used to filter the precipitates that gathered at the beaker's bottom and the filtrate was then dried at 50 °C for 2 hours.

The procedure was repeated for 100 ml, 150 ml and 200 ml, respectively. Up until characterisation, the produced electrodes and nanoparticles were kept in airtight bottles. Fig. 1 illustrates the chemical bath deposition (CBD) scheme adopted in the fabrication of the electrodes and nanoparticles. Various fabricated electrodes were used for electrochemical performances and SEM or energy dispersive X-ray spectroscopy (EDS) while powdered nanoparticles were employed for additional studies. Various samples were labelled and pH values indicated as presented in Table I.

TABLE I ELECTRODE LABELS AND PH VALUES

S/N	Electrodes	Label	pH value
1	Co_3O_4 @Mn O_2 @Zn $O/50$	CMZ/50	6.82
2	Co_3O_4 $@MnO_2$ $@ZnO/100$	CMZ/100	6.94
3	Co_3O_4 $@MnO_2$ $@ZnO/150$	CMZ/150	7.00
4	$Co_3O_4@MnO_2@ZnO/200$	CMZ/200	7.35

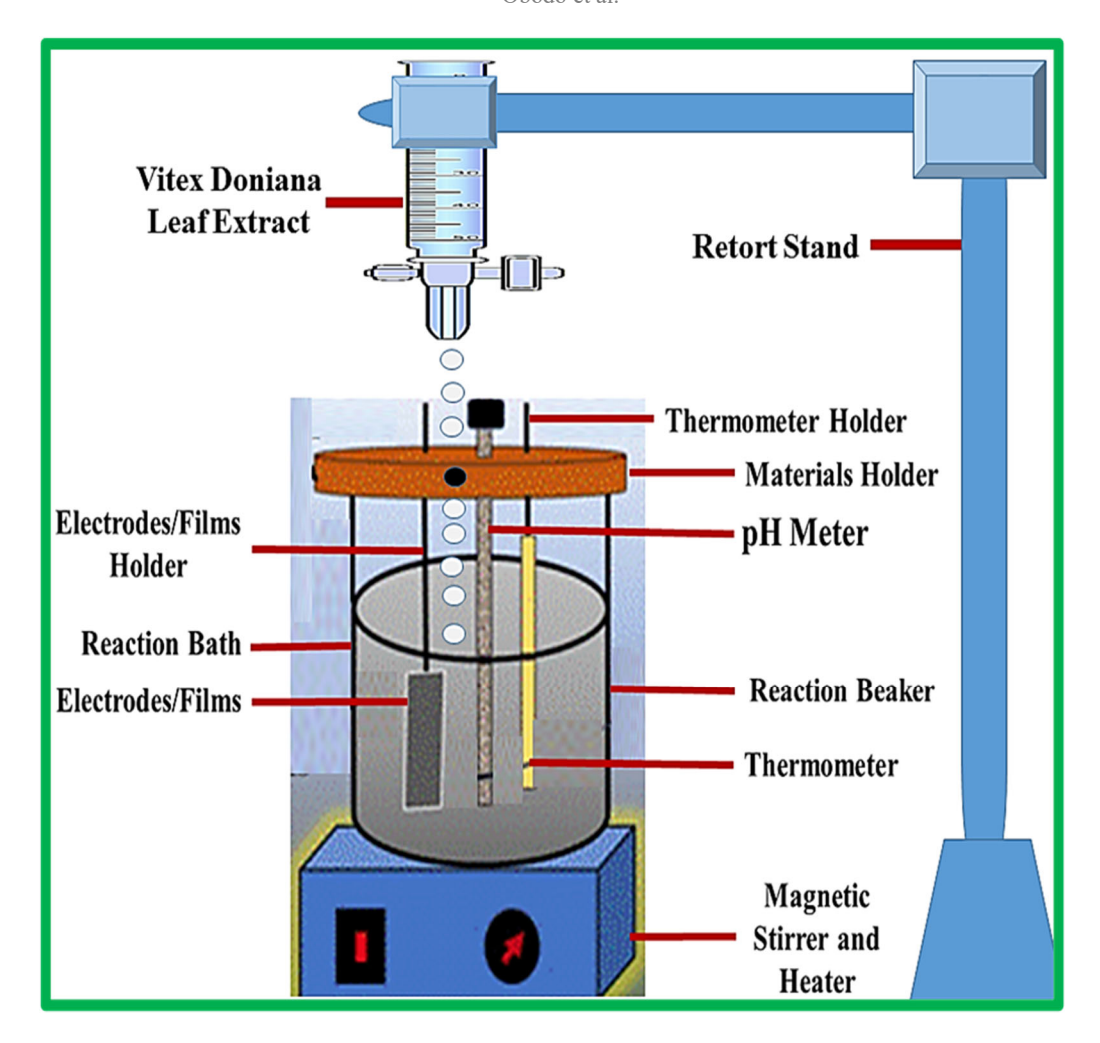


Fig. 1. Assembly 1: Chemical bath deposition scheme of electrodes and nanoparticles adapted from [32].

2.3 Characterising Constituents

The crystallographic facts and phase clarity of CMZ/50, CMZ/100, CMZ/150 and CMZ/200 electrodes were verified by X-ray diffraction (XRD), Advanced D8 Bruker, and by employing Cu-K α radiations (λ = 1.5418 Å). Various micro morphologies of these electrodes were detailed by field emission scanning electron microscopy (FESEM, JSM-6700F, JEOL). The optical characteristics of these electrodes were examined with a Double Beam Cary 5000 UV-Vis-NIR spectrophotometer.

2.4 Electrochemical Breakdown

The electrochemical assessments were investigated using a Gamry potentiostat CS350 model with 1.0 M sodium sulphate (Na₂SO₄) aqueous electrolytic solution. Various

features of CMZ/50, CMZ/100, CMZ/150 and CMZ/200 electrodes verified for electrochemical energy storage applications were attained by employing three electrode arrangements. CV, GCD and electrochemical impedance spectroscopy (EIS) were used to analyse the electrode arrangements.

3 Results and Discussion

3.1 X-Ray Diffraction Investigations

To estimate crystalline features and phases of CMZ/50 CMZ/100, CMZ/150 and CMZ/200 electrodes, which were enhanced by employing *Vitex doniana* leaf extract, XRD configuration was displayed in a 2θ range of 20–60° with a scan rate of 4° per minute as shown in Fig. 2. The XRD spectra of CMZ/50 CMZ/100, CMZ/150 and CMZ/200 electrodes matched with JCPDS card number 00-018-0408, which signified cobalt/manganese oxide with tetragonal crystal system, JCPDS card number 00-001-1149, which signified cobalt/zinc oxide with cubic crystal system, and JCPDS card number 00-024-1133, which signified manganese/zinc oxide with a tetragonal crystal system, respectively. These electrodes XRD spectra revealed 29.95°, 36.34°, 38.84°, 45.93°,49.48° and 56.40° with (hkl) reflection planes of (202), (311), (004), (400), (224) and (333) for cobalt/manganese oxide. Similarly, these electrodes revealed 36.34°, 38.84°, 45.93° and 56.40°, with (hkl) reflection planes of (111), (222), (400) and (422) for cobalt/zinc oxide. In addition, various electrodes displayed 29.95°, 36.34°, 38.84°, 44.79°, 49.48°, 54.44° and 56.40° with (hkl) reflection planes of (112), (211), (004), (220), (204), (312) and (303), for manganese/zinc, respectively.

Vitex doniana leaf extract phytochemicals triggered interactions and recombination of various transition metal ions, which resulted in co-existence and matching of various peaks at $2\theta = 36.34^{\circ}$, 38.84° , 45.95° and 56.40° . These, in turn, resulted in more crystalline nature and enhancement of various properties. Various high-pitched and renowned peaks of various electrodes designate the high crystalline nature of the fabricated nanoparticles and electrodes. It was observed that an electrode with the pH at neutral (7) has the best crystalline nature compared to other electrodes. At the CMZ/150 sample with the pH of neutral, the *Vitex doniana* leaf extract phytochemicals triggered interactions and recombination of various transition metal ions at neutral medium, which resulted in an enhanced synergistic and co-existence among various ions, and therefore delivered a better performance compared to other combinations.

Equation 1 of the Debye-Scherer equation was used to determine the crystalline sizes of these electrodes [33].

$$D = \frac{k\lambda}{\beta \cos \theta} \tag{1}$$

where λ denotes the wavelength, approximately 1.5418 Å, k is the Debye-Scherer's constant, D is the crystalline size, β is the full width at half maximum of major peak intensities in radians, and θ is the Bragg's angle in degrees.

Table II presents the computed crystalline sizes for of CMZ/50 CMZ/100, CMZ/150 and CMZ/200 electrodes.

TABLE II CRYSTALLINE SIZE OF NANOPARTICLES

Electrodes	D (Crystalline size) nm
CMZ/50	40.95
CMZ/100	35.72
CMZ/150	31.74
CMZ/200	37.83

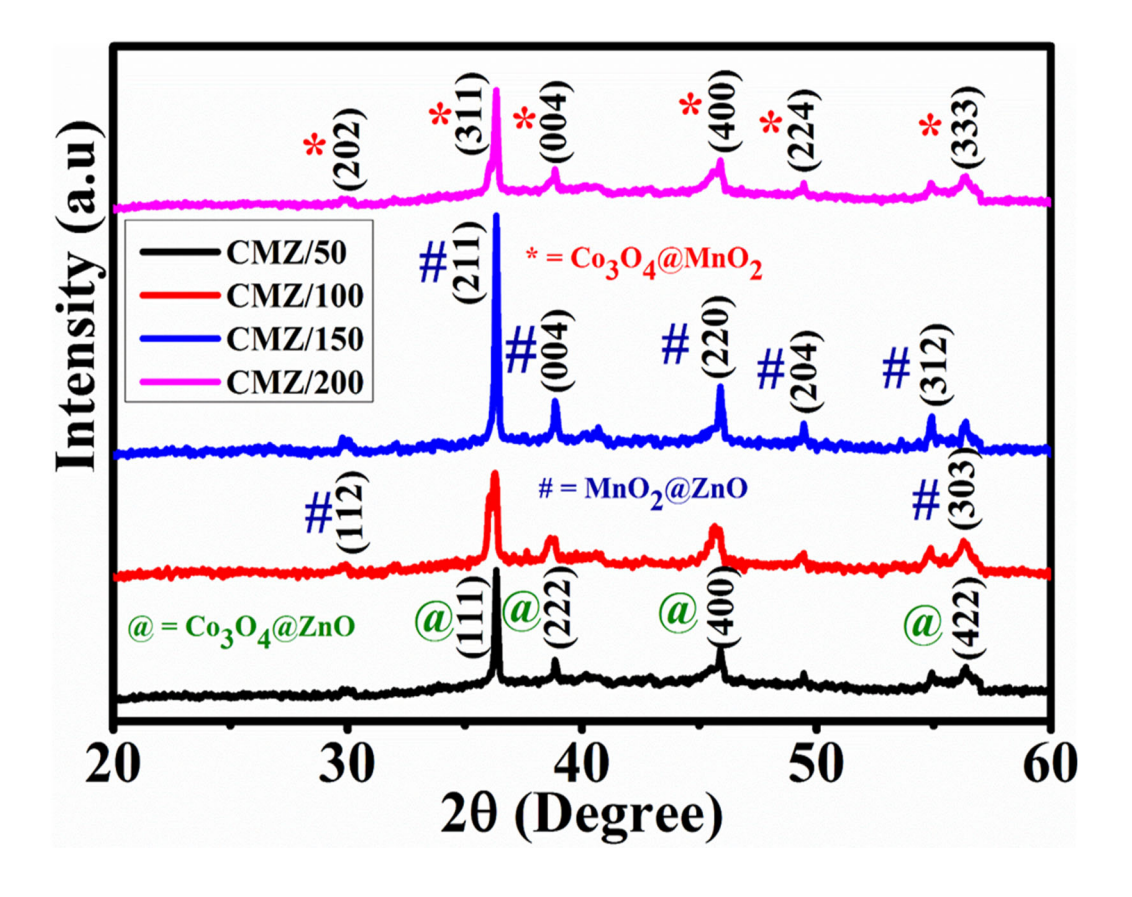


Fig. 2. XRD spectra of CMZ/50 CMZ/100, CMZ/150 and CMZ/200 electrodes enhanced by employing *Vitex doniana* leaf extract.

3.2 Morphology Examination

Scanning electron microscopy (SEM) explanations of the invented CMZ/50 CMZ/100, CMZ/150 and CMZ/200 electrodes were exposed as contained in Fig. 3(a–d) congruently. Fig. 3(a) (CMZ/50) shows a mixture of evenly distributed nanospheres and agglomerated nanospheres. These aggregate-like and irregular spherical nanoparticles of different sizes agglomerated at several points. Fig. 3(b) (CMZ/100) shows nanospherical, nano quasi-spherical and some irregular flaky nanoparticles mostly agglomerated at numerous positions on the electrode surfaces. Fig. 3(c) (CMZ/150) shows densely agglomerated nanospherical, nano flaky-like assemblies and nano quasi-rod-like nanoparticles, crowded at numerous locations in a compressed routine within electrodes surfaces. Fig. 3(d) (CMZ/200) shows thickly globular, spherical, quasi-globular and spherical as well as quasi-rod-like nanoparticles with irregular proportions in miniature agglomerations at some places within electrode surfaces. These miniature particles present in various electrodes proliferate the speed by which electrons stream among electrodes and electrolytic solution, which generate more conductive channels for integration.

Vitex doniana constituents' phytochemicals prompted the creation of tiny particles, and enhanced synergistic effects among various transition metallic ions, consequently increasing the crystallinity of various electrodes as well as their specific capacitance, energy density and power density [3], [34]–[36]. As observed in the XRD results, electrodes with pH at neutral (7) possess numerous shapes and sizes of nanoparticles heavily packed together, which indicate more crystallinity compared to other electrodes. These provide better performance compared to the other electrodes.

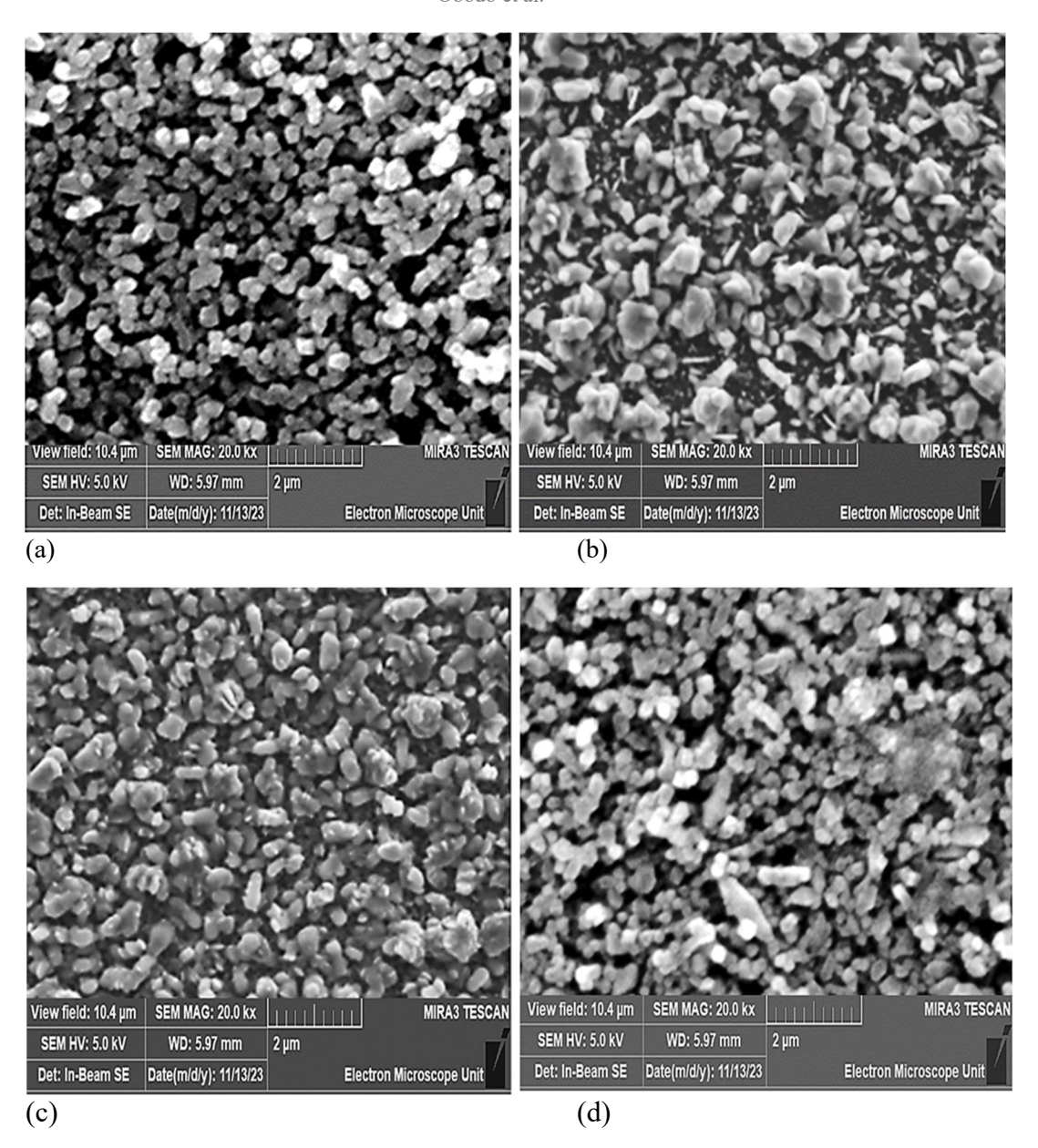


Fig. 3. SEM imageries of (a) CMZ/50, (b) CMZ/100, (c) CMZ/150 and (d) CMZ/200 electrodes.

3.3 Investigation of Elemental Constituents of CMZ/150 Electrode

The elemental configurations of the invented CMZ/150 electrode enhanced with *Vitex doniana* leaf extract are additionally established by EDS analysis in Fig. 4(a). The existence of Co, Mn, Zn, O, Fe, P and Si were detected. The occurrence of Fe, P and Si elemental crests is possibly the result of the addition of *Vitex doniana* leaf extract used in the course of the invention of this electrode. The larger percentages of Co, Mn and Zn elements witnessed in the CMZ/150 electrode are beneficial for rapid redox reactions. A bloated measure of oxidations/reductions reactions of ions offered by Co⁺, Mn⁺ and Zn⁺ ions empowers amplified electrode conductivities, and occasions in lesser charges conduction period and improved specific capacitances, energy and power densities as well as cycle firmness [37]. Elemental dispersal in CMZ/150 electrode was also acknowledged by the EDS investigation as reported by the XRD.

The Fourier transform infrared spectroscopy (FTIR) analysis of invented CMZ/150 electrode material was conducted within the segment of immersion in the intermediate of 500 cm⁻¹–4 000 cm⁻¹ wavelengths range equally accessible inside as shown in Fig. 4(b). Various perceived pinnacles between 1 031 cm⁻¹–1 036 cm⁻¹ approve the meandering feature of carbon/oxygen molecular interactions [38], [39]. Peaks detected within 1 040 cm⁻¹–1 550 cm⁻¹ signify immersed complexes referred to as aromatic ring [40]. In addition, peaks witnessed within 2 961 cm⁻¹–2 971 cm⁻¹ indicate an elongation of methyl and alkynes assemblies whereas crests within 3 076 cm⁻¹–3 659 cm⁻¹ represent the broadening of oxygen/hydrogen intermolecular [41]–[43].

The general FTIR outcome demonstrates the existence of metallic oxides plus water molecules within nanoparticles and electrodes synthesised, supportive of XRD analysis and validates the growth of CMZ/150 facilitated *Vitex doniana* leaf extracts electrode material. Table III presents the existence and various locations of functional collections present inside the invented CMZ/150 facilitated by *Vitex doniana* leaf extract electrode material.

TABLE III
FTIR BREAKDOWN OF CMZ/150 FACILITATED SARCOPHRYNIUM
BRACHYSTACHYS LEAF EXTRACT ELECTRODE

S/N	S/N Wave number Vibrational (cm ⁻¹) modes		Functional group
1	1 032-1 040	Meandering	Carbon/oxygen (C-O-C) [38], [39]
2	1 401–1 551	Twisting	Aromatic rings [40], [44]
3	2962 - 2972	Elongating	Methyl (C-H) plus alkynes (C≡C) groups
4	3 077 – 3 660	Broadening	H-O-H (hydroxyl compounds)

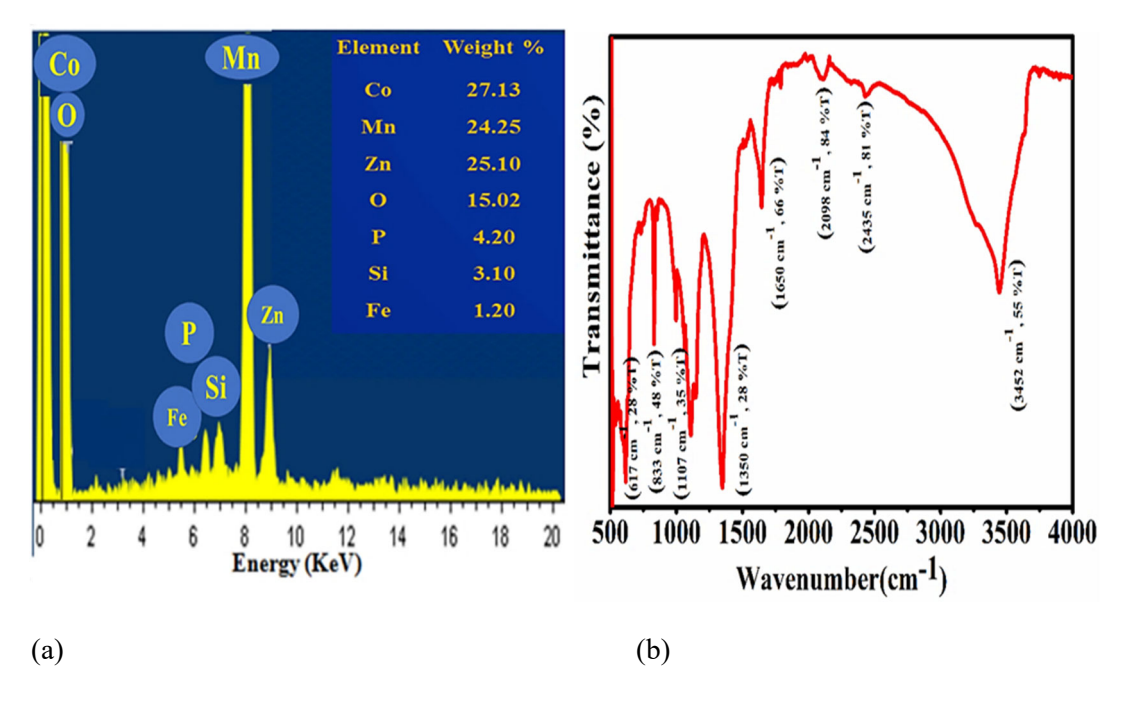


Fig. 4. (a) EDS and (b) FTIR of CMZ/150 electrode.

3.4 Optical Evaluation

The UV-Vis-NIR optical absorption spectrum of CMZ/50 CMZ/100, CMZ/150 and CMZ/200 electrodes enhanced with *Vitex doniana* leaf extract are shown in Fig. 5(a). CMZ/50 CMZ/100, CMZ/150 and CMZ/200 electrodes disclosed small peaks within 280.00–310.00 nm. Peaks within this region signify absorptions from flavonoid and its products [45]. CMZ/50 CMZ/100, CMZ/150 and CMZ/200 electrodes have small absorbances oscillating within 0.13 a.u. to 0.05 a.u. These properties of small absorbance have transpired within visible sections of the spectrum and extend to nearinfrared areas, which demonstrate higher transmittance features of CMZ/50 CMZ/100, CMZ/150 and CMZ/200 electrodes. The absorbance spectrum of CMZ/50 amplified beginning at 0.12 a.u. to 0.13 a.u. contained in a visible area then drop constantly towards an infrared section to 0.05 a.u. CMZ/100 electrode followed CMZ/50 steps by increasing from 0.10 a.u. to 0.11 a.u. and abridged to 0.06 a.u. within a near-infrared segment. In addition, the CMZ/150 electrode trailed the identical trend, intensified from 0.06 a.u. to 0.09 a.u. and abridged to 0.05 a.u. within an infrared section. CMZ/200 electrode absorbance enlarged from 0.06 to 0.09 a.u. and condensed to 0.05 a.u. in the infrared section. CMZ/150 electrode with pH of 7 (neutral) absorbance values were averaged, which portrays reciprocated co-existence and interfaces of CMZ/50 CMZ/100 and CMZ/150 electrodes, and depicts an extended interactions among various constituent ions.

Fig. 5(b) shows the energy band gaps of CMZ/50 CMZ/100, CMZ/150 and CMZ/200 electrodes. These energy band gaps were valued by engaging Equation 2 [23].

$$(\alpha h \nu) = A (E_g - h \nu)^n \tag{2}$$

where α signifies the absorption coefficient, E_g represent the energy band gap, A denotes the constant and $n = \frac{1}{2}$ for straight allowable transitions, respectively.

CMZ/50 CMZ/100, CMZ/150 and CMZ/200 electrode energy band gaps were estimated using plots of $(\alpha h v)^2$ versus photons energies (hv). CMZ/50 CMZ/100, CMZ/150 and CMZ/200 electrodes possess band gap energies of 2.60 eV, 2.50 eV, 2.10 eV and 2.40 eV, respectively. The energy band gaps results displayed a reduction at CMZ/150 electrode with the pH value at 7 (neutral). The observed reduction can be credited to active co-existence and collaborations of these metal ions in CMZ/150 electrode with pH 7, which stimulate heightened crystallinity [46].

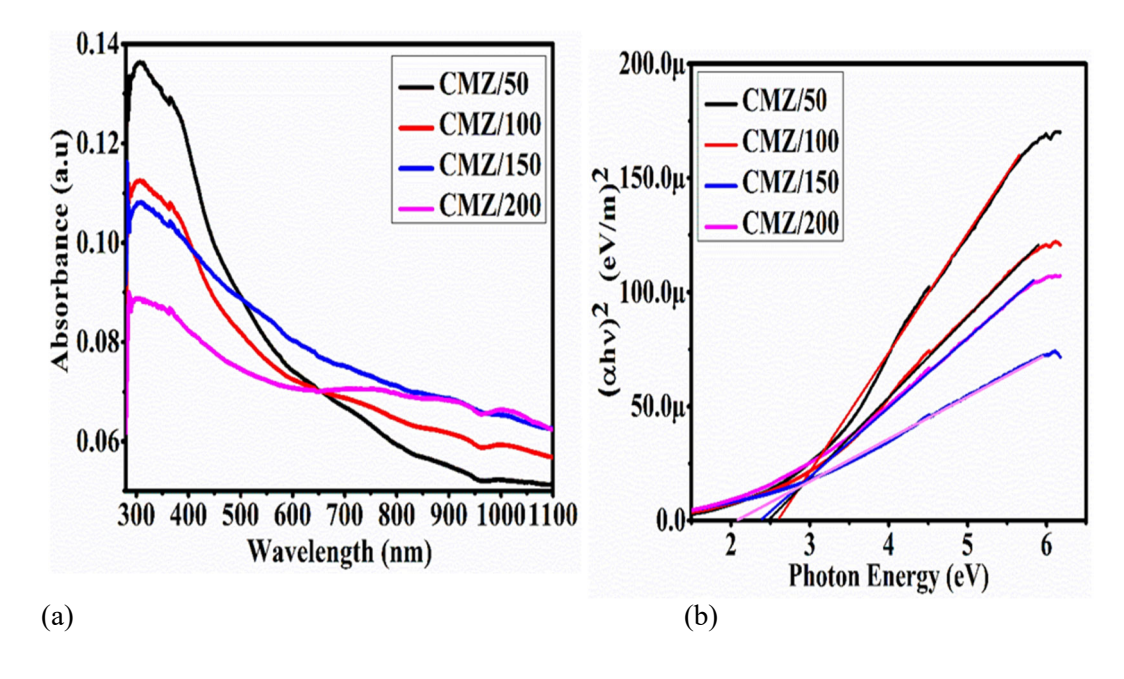


Fig. 5. (a) Absorbance and (b) Energy band gaps of CMZ/50, CMZ/100, CMZ/150 and CMZ/200 electrodes.

3.5 Electrochemical Estimations

CMZ/50, CMZ/100, CMZ/150 and CMZ/200 electrodes were estimated by engaging CV, GCD and EIS. The best performing potential window for CMZ/50, CMZ/100, CMZ/150 and CMZ/200 electrodes were verified, and conventionally established to perform better between 0.00 and 0.70 V. Consequently, CV patterns developed for

CMZ/50, CMZ/100, CMZ/150 and CMZ/200 electrodes are displayed in Fig. 6(a-d). CMZ/50, CMZ/100, CMZ/150 and CMZ/200 electrodes were studied using amendable scan rates stretching between 1.0–10.0 mV/s range. The results presented the absence of quadrilateral curvatures in CV curves of these electrodes portraying the pseudocapacitive nature of CMZ/50, CMZ/100, CMZ/150 and CMZ/200 electrodes [47]. The transferrable oxidation prominences of cobalt (C⁺³) and manganese (Mn⁺²) are typically accountable for revocable responses in the inner CV patterns as shown in Fig. 6(a-d) [48]. The various results indicate that the combination of Co₃O₄, MnO₂ and ZnO in CMZ/50, CMZ/100, CMZ/150 and CMZ/200 electrodes meaningfully enhances CV areas, which demonstrate a vigorous integration of Co⁺, Mn⁺ and Zn⁺ ions as presented in Fig. 6(a-d). This reflection can be ascribed to the shortened volume of dissolutions of metallic ions inside electrolytic solutions, which enhance the conductivities, similarly affirmed by He et al. [49] and Arshad et al. [50]. However, apart from shifts in redox crests within anodic and cathodic potentials, no distinct transformation in the CV curves was perceived at advanced scan rates. These changes could be brought on by electrochemical immersion and separations within the electrolytic solution [51]. The obvious capacitances of CMZ/50, CMZ/100, CMZ/150 and CMZ/200 electrodes were estimated by employing Equation 3 [52].

$$C_{sp} = \frac{1}{mVs} \int i(V)dV \left(\frac{F}{g}\right) \tag{3}$$

where m represents the energetic mass (mg), V signifies the utilised potential window (Volts), S symbolises the scan rates applied (mV/s) and i signifies the adopted current (A).

The evaluated specific capacitances of CMZ/50, CMZ/100, CMZ/150 and CMZ/200 electrodes engaging a 1.0 mV/s scan rate, displayed peak specific capacitance of 785, 1 038, 1 215 and 982 F/g for the CMZ/50, CMZ/100, CMZ/150 and CMZ/200 electrodes, respectively.

The rise in the specific capacitance assessment of CMZ/150 electrode can be attributed to the superior apparent area, the higher penetrability of CMZ/150 electrode prompted by the neutrality of the solution and the presence of various phytochemicals in *Vitex doniana* leaf extract [49]. Obodo *et al.* [52] reported that enhanced morphologies and crystalline features increase uniform interactions between electrodes and electrolytic solutions, hence, enlarged specific capacitances. The various phytochemicals in *Vitex doniana* leaf extract triggered enhanced interactions between the constituents' ions and electrolytic ions, consequently prompting a better performance for various electrodes.

The EIS analysis was adopted in estimating the accessible resistances and charging mechanisms presented by these electrodes, by varying the frequency from 0.00 to 100.00 kHz. As demonstrated in Fig. 6(e), Nyquist schemes are executed between real impedance (Z') and imaginary impedance (Z''). Various electrodes display non-existent semi-circles, which indicate small resistances and high conductivities [53].

CMZ/50, CMZ/100, CMZ/150 and CMZ/200 electrodes had equivalent series resistances (ESRs) of 0.46 Ω , 0.55 Ω , 0.36 Ω and 0.72 Ω correspondingly. The CMZ/200 electrode possesses maximum ESR worth, which may be related to the electrodes high resistive boundaries [54]. However, the CMZ/150 electrode possesses the lowest resistance value, which illustrates an exceptionally conductive property, validated by CV results. The ESR represents the combined impacts of solution resistance, electrode/electrolyte borders and electrode resistance. The hydrous characteristic nature of CMZ/50, CMZ/100, CMZ/150 and CMZ/200 provided additional networks for the passage of electrons and ions, motivated by Vitex doniana leaf extract arbitrated electrode by providing enough hydroxide ions (OH-1) enhancing cooperation with various ions within electrode openings [55]. The EIS plots associated with the distribution of ions for various electrodes are shown in Fig. 6(e). The model circuit used in calculating various parameters consists of the constant phase elements, Warburg impedance; charges transfer resistances, solutions resistances represented as R_s, R_{ct}, W and Q respectively as shown as an inset in Fig. 6(e) respectively, with their varied values presented in Table IV.

TABLE IV ASSESSED MEASURES OF R_s , R_{ct} , W, AND Q FOR VARIOUS FABRICATED ELECTRODES

S/N	Electrodes	R _s	R _{ct}	W	Q (-(90*n))
		(Ω)	(Ω)	(ohm cm ²)	degree, where $n = 1$
1	CMZ/50	0.08	9.10	0.50	0.60
2	CMZ/100	0.06	8.24	0.40	0.58
3	CMZ/150	0.05	6.00	0.35	0.45
4	CMZ/200	0.13	10.40	0.72	0.64

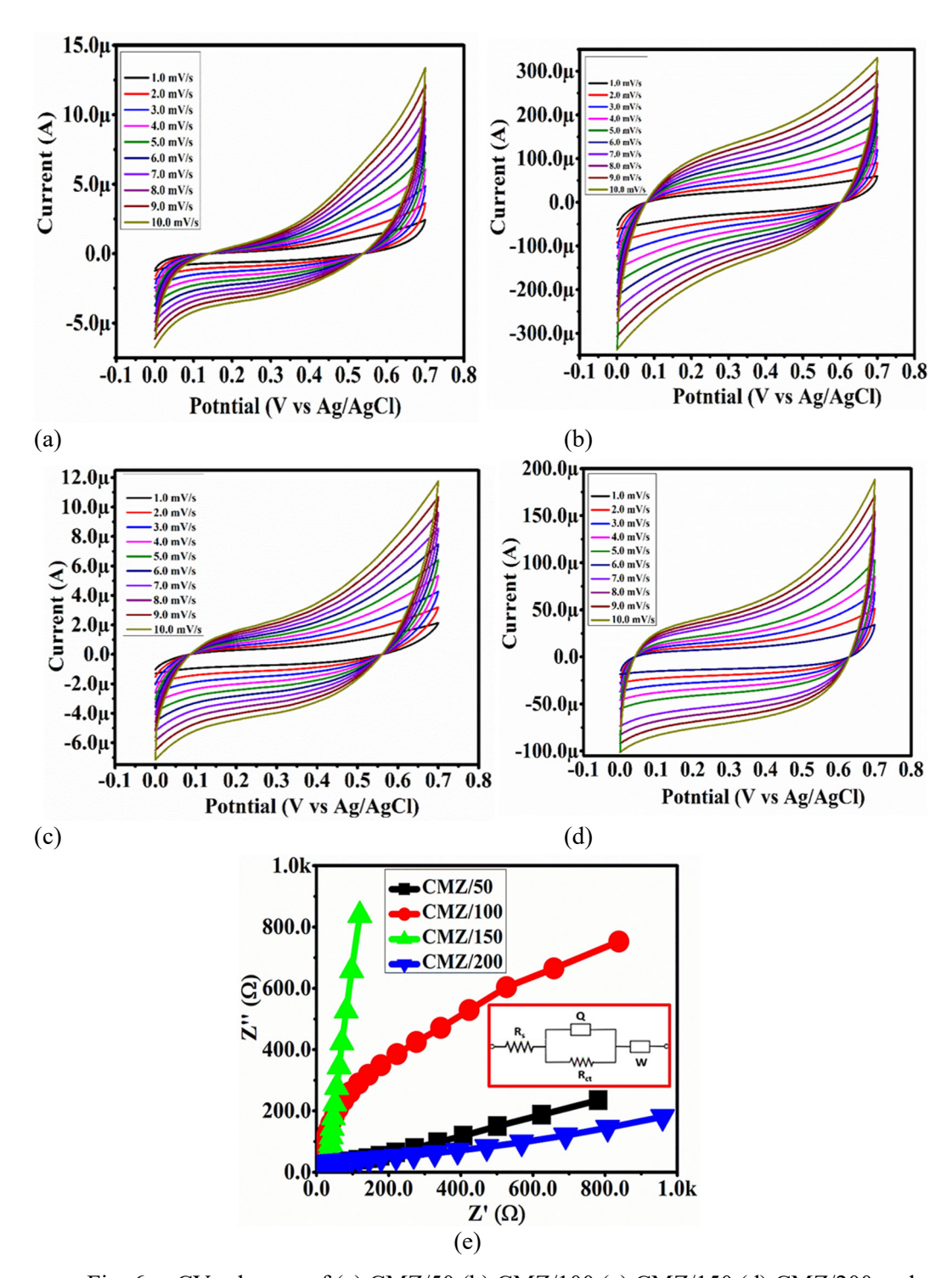


Fig. 6. CV schemes of (a) CMZ/50 (b) CMZ/100 (c) CMZ/150 (d) CMZ/200 and (e) EIS of various electrodes with the CPE model in the enclosure.

Fig. 7(a) and (b) depict the GCD relative curves for the electrodes CMZ/50, CMZ/100, CMZ/150 and CMZ/200 at 0.5 A/g and 1.0 A/g current densities, respectively. The specific capacitances assessed for CMZ/50, CMZ/100, CMZ/150 and CMZ/200 electrodes at 0.5 A/g and 1.0 A/g are 978, 1 012, 1 250, 879 and 928, 994, 1 138, 850 F/g, respectively. The findings of this GCD evaluation concurred with the report by Obodo *et al.* [56] in a study about Co₃O₄@CuO@NiO composite electrodes for supercapacitor applications. These GCD results also indicate that the CMZ/150 electrode performed better than the other electrodes at different current densities, which indicates a longer discharge time and a greater specific capacitance. This might be linked to improved morphology and crystallinity as a result of increased interactions among multiple ions in the system brought about by an increase in the number of distinct ions and phytochemicals [3].

GCD investigations discovered that, maybe as the result of rapid charge and discharge rates, capacitance values decrease with higher current densities (1.0 A/g). However, research [52], [57] has indicated that excessive active material consumption occurs at low current densities, which extend the time it takes for electrolytic ions to penetrate the interior section of the materials and attract larger specific capacitances for different electrodes [1]. In addition, it is noted that the CMZ/150 electrode's microstructure, which consists of densely agglomerated nano spherical shaped, nano flaky-like assemblies, and nano quasi-rod-like nanoparticles, is highly suitable for the stress-free availability of electrolytic ions. This leads to increased supercapacitive performances. These nanoparticles are crowded at various locations in a compressed routine within electrode surfaces [58], [59]. Equations (4) and (5) were used to determine the energy (E_d) and power (P_d) densities of the CMZ/50, CMZ/100, CMZ/150, and CMZ/200 electrodes, respectively [1].

$$E_{d} = 0.5 \times C_{s} (\Delta V)^{2} \tag{4}$$

$$P_d = 3.6 \frac{E_D}{T_d} \tag{5}$$

where, E_d represents energy density, ΔV signify potential window and T_d denotes time to discharge.

Energy densities evaluated for CMZ/50, CMZ/100, CMZ/150 and CMZ/200 electrodes at 0.50 A/g and 1.00 A/g stood at 239.61, 247.94, 306.25, 215.36 Wh/kg and 227.36, 243.53, 278.81, 199.75 Wh/kg correspondingly. Voltage reductions have been detected at given positions within GCD schemes. These voltage drops may be credited to energy wastages within electrodes owing to the existence of resistances [60]. Various power densities measured for CMZ/50, CMZ/100, CMZ/150 and CMZ/200 electrodes at 0.5 A/g and 1.0 A/g are 18.45, 16.85, 25.66, 13.77 W/kg and 17.33, 18.66, 22.9, 12.11 W/kg, respectively. The columbic efficiency for 10 000 cycles was calculated using the CMZ/150 electrode, which shows better performance compared to other

electrodes. Using Equation 6 [3], the columbic efficiency of CMZ/150 electrode was determined.

Columbic efficiency
$$(\eta) = \frac{\Delta t_d}{\Delta t_c} \times 100\%$$
 (6)

where Δt_d and Δt_c are changes in discharging and charging time.

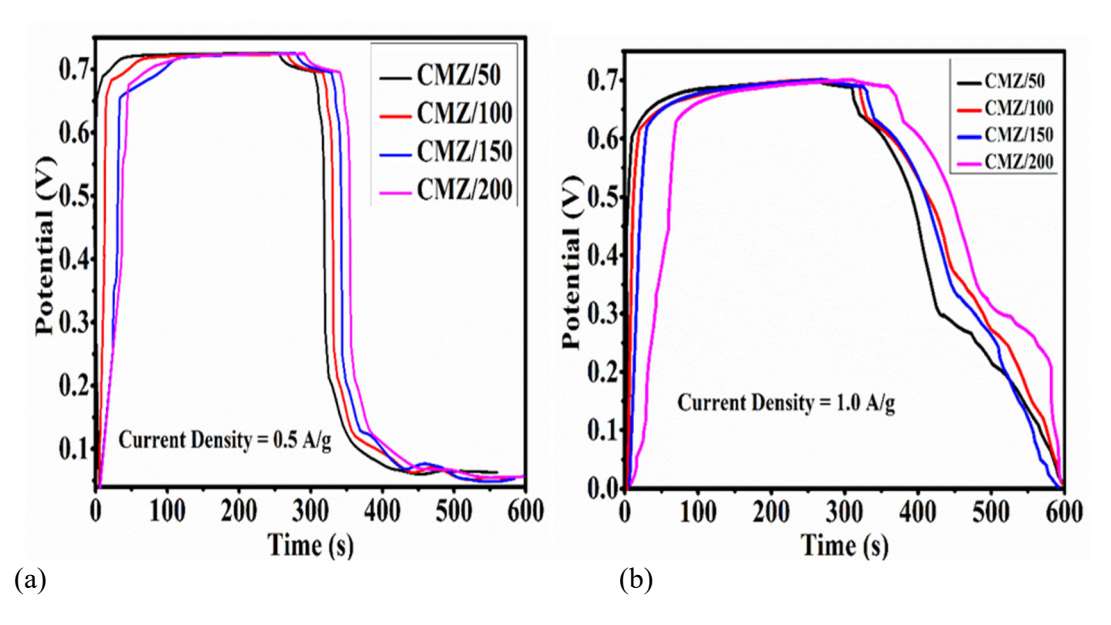


Fig. 7. Patterns of (a) 0.5 A/g and (b) 1.0 A/g GCD of CMZ/50, CMZ/100, CMZ/150 and CMZ/200 electrodes.

The CMZ/150 electrode cycling analysis is shown in Fig. 8. The cycle analysis denotes a cycle stability of 97.25% skill after undertaking 10 000 cycles. Plotting the GCD outlines of the last 20 full series which changed somewhat as cycling progressed and demonstrated the remarkable cyclic reversibility of CMZ/150 electrode material shown as an inset in Fig. 8 [61]–[64].

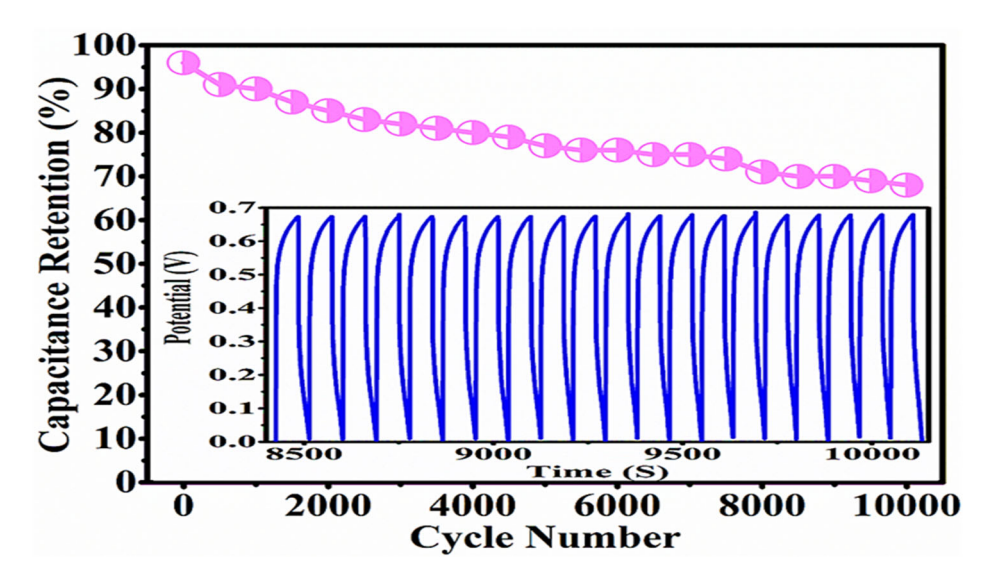


Fig. 8. Stability investigation outlines of CMZ/150 electrode.

4 Conclusion

The use of *Vitex doniana* leaf extract as the reducing agent for CMZ/50, CMZ/100, CMZ/150 and CMZ/200 electrodes is created on FTO substrates by the use of the CBD process. The phytochemicals found in *Vitex doniana* leaf extract affect the morphologies, crystallinities, metal oxide reaction kinetics and supercapacitive performances of different fabricated electrodes. In addition to displaying a maximum specific capacitance of 1 215 F/g from CV, 1 250 and 1 138 F/g at 0.5 and 1.0 A/g from GCD findings, the more performant CMZ/150 electrode also provided 97.5% retention capacity across 10 000 full cycles.

Cobalt, manganese and zinc oxides work synergistically to produce an improved energy-storing electrode, which is the reason for the remarkable performance of the CMZ/150 electrode. Strong bonding to the FTO substrates without binders was induced by the high surface area for electrolytic ion intercalation and deintercalation provided by the presence of several phytochemicals in the *Vitex doniana* leaf extract. Owing to the increasing quantity of distinct various salt ions and phytochemicals that promoted more interactions among diverse ions and caused improved shape and crystallinity, it also stimulated higher interfaces among constituent ions in the system, which result in an enriched performance. The CMZ electrodes delivered an extraordinary performance, which indicate that they are good candidates for supercapacitor electrodes materials. We suggest adopting the leaf extract of different plants using the same technique for future research.

5 Author Contributions

RMO, HEN, SCE and JNA synthesised the nanomaterials, fabricated various electrodes, carried out the characterisations and analysed the results. SEU, CUE, MOD and UCR worked on the manuscript's editing. The data were conceptualised, proofread and confirmed by IA and MM.

6 Acknowledgements

RMO and IA acknowledges the award of the NCP-UNESCO-TWAS Postdoctoral Fellowship. RMO acknowledges the award of the UNISA (SIRGS and CGS) Postdoctoral Fellowship. RMO also acknowledges the grant by the TETFUND under IBR contract number TETFUND/DR&D/CE/UNI/UMUAGWO/IBR/2022/VOL.1#22.

7 Data Availability

The authors confirm that the data supporting the findings of this study are available from the corresponding author upon reasonable request.

8 References

- [1] R. M. Obodo *et al.*, "Effects of copper ion irradiation on Cu_yZn_{1-2y-x}Mn_y/GO supercapacitive electrodes," *J. Appl. Electrochem.*, vol. 51, pp. 829–845, Mar. 2021, doi: 10.1007/s10800-021-01543-3.
- [2] L. Li, Z. A. Hu, N. An, Y. Y. Yang, Z. M. Li and H. Y. Wu, "Facile Synthesis of MnO₂/CNTs Composite for Supercapacitor Electrodes with Long Cycle Stability," *J. Phys. Chem. C*, vol. 118, no. 40, pp. 22865–22872, Sept. 2014, doi: 10.1021/jp505744p.
- [3] R. M. Obodo, H. E. Nsude, S. C. Ezike, C. Ononogbo, I. Ahmad, M. Maaza and F. I. Ezema, "Exploring dual synergistic effects of CeO₂@ZnO mediated sarcophrynium brachystachys leaf extract nanoparticles for supercapacitor electrodes applications," *Hybrid Adv.*, vol. 5, p. 100143, Apr. 2024, doi: 10.1016/j.hybadv.2024.100143.
- [4] T. Brousse, D. Bélanger and J. W. Long, "To Be or Not To Be Pseudocapacitive?," *J. Electrochem. Soc.*, vol. 162, no. 5, p. A5185, Mar. 2015, doi: 10.1149/2.0201505jes.
- [5] R. M. Obodo, A. C. Nwanya, I. S. Ike, I. Ahmad and F. I. Ezema, "Role of Carbon Derivatives in Enhancing Metal Oxide Performances as Electrodes for Energy Storage Devices," in *Chemically Deposited Nanocrystalline Metal Oxide Thin Films*, F. I. Ezema, C. D. Lokhande and R. Jose, Eds, Cham. Cham, Springer, 2021, pp. 469–488, doi: 10.1007/978-3-030-68462-4_18.
- [6] Y. Zhu, L. Peng, D. Chen and G. Yu, "Intercalation Pseudocapacitance in Ultrathin VOPO₄ Nanosheets: Toward High-Rate Alkali-Ion-Based Electrochemical Energy Storage," *Nano Lett.*, vol. 61, no. 1, pp. 742–747, Dec. 2016, doi: 10.1021/acs.nanolett.5b04610.

- [7] R. M. Obodo *et al.*, "Radiations Induced Defects in electrode materials for energy storage devices," *Radiat. Phys. Chem.*, vol. 191, p. 109838, Feb. 2022, doi: 10.1016/j.radphyschem.2021.109838.
- [8] R. Dubey and V. Guruviah, "Review of carbon-based electrode materials for supercapacitor energy storage," *Ionics*, vol. 25, no. 4, pp. 1419–1445, Feb. 2019, doi: 10.1007/s11581-019-02874-0.
- [9] R. M. Obodo *et al.*, "Performance optimization of bimetallic Co₃(PO₄)₂@Ni₃(PO₄)₂ electrodes for supercapacitive applications," *J. Mater. Sci: Mater. Electron.*, vol. 35, p. 351, Feb. 2024, doi: 10.1007/s10854-024-12079-5.
- [10] B. K. Kim, S. Sy, A. Yu and J. Zhang, "Electrochemical Supercapacitors for Energy Storage and Conversion," in *Handbook of Clean Energy Systems*, John Wiley & Sons, 2015, doi: 10.1002/9781118991978.hces112.
- [11] R. M. Obodo, A. C. Nwanya, I. Ahmad, M. A. Kebede and F. I. Ezema, "Carbon Derivatives in Performance Improvement of Lithium-Ion Battery Electrodes," in *Electrode Materials for Energy Storage and Conversion*, A. M. Kebede and F. I. Ezema, Taylor & Francis, CRC Press, 2021, pp. 23–33, doi: 10.1201/9781003145585-2.
- [12] S. J. Ding, T. Zhu, J. S. Chen, Z. Y. Wang, C. L. Yuan and X. W. Lou, "Controlled synthesis of hierarchical NiO nanosheet hollow spheres with enhanced supercapacitive performance," *J. Mater. Chem.*, vol. 21, pp. 6602–6606, 2011, doi: 10.1039/c1jm00017a.
- [13] W. Li *et al.*, "Facile synthesis of three-dimensional structured carbon fiber-NiCo₂O₄-Ni(OH)₂ high-performance electrode for pseudocapacitors," *Sci. Rep.*, vol. 5, pp. 9277–9282, Mar. 2015, doi: 10.1038/srep09277.
- [14] C. Z. Yuan *et al.*, "Large-scale Co₃O₄ nanoparticles growing on nickel sheets via a one-step strategy and their ultra-highly reversible redox reaction toward supercapacitors," *J. Mater. Chem.*, vol. 45, pp. 18183–18185, 2011, doi: 10.1039/c1jm14173b.
- [15] L. Cao, F. Xu, Y. Y. Liang and H. L. Li, "Preparation of the Novel Nanocomposite Co(OH)₂/Ultra-Stable Y Zeolite and Its Application as a Supercapacitor with High Energy Density," *Adv. Mater.*, vol. 16, no. 20, pp. 1853–1857, Oct. 2004, doi: 10.1002/adma.200400183.
- [16] J. M. Song *et al.*, "One-pot synthesis of ZnO decorated with AgBr nanoparticles and its enhanced photocatalytic properties," *Cryst. Eng. Comm.*, vol. 13, pp. 2652–2659, 2014, doi: 10.1039/c3ce41943f.
- [17] J. M. Song, S. S. Zhang and S. H. Yu, "Multifunctional Co_{0.85}Se-Fe₃O4 Nanocomposites: Controlled Synthesis and Their Enhanced Performances for Efficient Hydrogenation of *p*-Nitrophenol and Adsorbents," *Small*, vol. 10, no. 4, pp. 717–724, Feb. 2014, doi: 10.1002/smll.201301386.

- [18] C. Li, S. Bolisetty and R. Mezzenga, "Hybrid Nanocomposites of Gold Single-Crystal Platelets and Amyloid Fibrils with Tunable Fluorescence," *Adv. Mater.*, vol. 25, no. 27, pp. 3694–3700, Jul. 2013, doi: 10.1002/adma.201300904.
- [19] J. Zhang, J. M. Song, H. L. Niu, C. J. Mao, S. Y. Zhang and Y. H. Shen, "ZnFe₂O₄ nanoparticles: Synthesis, characterization, and enhanced gas sensing property for acetone," *Sens. Actuator B-Chem.*, vol. 221, pp. 55–62, Dec. 2015, doi: 10.1016/j.snb.2015.06.040.
- [20] Y. Jiao, J. Liu, B. S. Yin, S. W. Zhang, F. Y. Qu and X. Wu, "Hybrid α-Fe₂O₃@NiO heterostructures for flexible and high performance supercapacitor electrodes and visible light driven photocatalysts," *Nano Ener.*, vol. 10, pp. 90–98, Nov. 2014, doi: 10.1016/j.nanoen.2014.09.002.
- [21] D. Cai *et al.*, "High-Performance Supercapacitor Electrode Based on the Unique ZnO@Co₃O₄ Core/Shell Heterostructures on Nickel Foam," *ACS Appl. Mater. Interfaces*, vol. 6, no. 18, pp. 15905–15912, Aug. 2014, doi: 10.1021/am5035494.
- [22] M. Maaza *et al.*, "Peculiar Size Effects in Nanoscaled Systems," *Nano-Horizons*, vol. 1, no. 1, pp. 1–36, Jul. 2022, doi: 10.25159/NanoHorizons.9d53e2220e31.
- [23] R. M. Obodo *et al.*, "Evaluation of 8.0 MeV Carbon (C²⁺) Irradiation Effects on Hydrothermally Synthesized Co₃O₄-CuO-ZnO@GO Electrodes for Supercapacitor Applications," *Electroanal.*, vol. 32, no. 12, pp. 2958–2968, Dec. 2020, doi: 10.1002/elan.202060382.
- [24] A. O. Juma, E. A. A. Arbab, C. M. Muiva, L. M. Lepodise and T. G. Mola, "Synthesis and characterization of CuO-NiO-ZnO mixed metal oxide nanocomposite," *J. Alloys Compd*, vol. 723, pp. 866–872, Nov. 2017, doi: 10.1016/j.jallcom.2017.06.288.
- [25] M. H. Habibi and B. Karimi, "Fabrication and Characterization of CuO-ZnO-Cu₂O Nano-Composites by Sol-Gel Route: Effect of Calcinations Temperature," Syn. React. Inorg. Metaorg. Nanometal Chem., vol. 44, no. 9, pp. 1358–1362, 2014, doi: 10.1080/15533174.2013.801858.
- [26] R. M. Obodo *et al.*, "Annealing optimization of graphitized Co₃O₄@CuO@NiO composite electrodes for supercapacitor applications," *Energy Storage*, vol. 4, no. 5, p. e347, Oct. 2022, doi: 10.1002/est2.347.
- [27] L. Dinan, N. Z. Mamadalieva and R. Lafont, "Dietary Phytoecdysteroids," in *Handbook of Dietary Phytochemicals*, J. Xiao, S. Sarker and Y. Asakawa, Eds., Singapore: Springer, 2019, pp. 1–54, doi: 10.1007/978-981-13-1745-3 35-1.
- [28] J. C. Okafor, "Development of forest tree crops for food supplies in Nigeria," *For. Ecol. Manag.*, vol. 1, pp. 235–247, 1976–1977, doi: 10.1016/0378-1127(76)90028-1.
- [29] J. C. Okafor, "Edible indigenous woody plants in the rural economy of the Nigerian forest zone," For. Ecol. Manag., vol. 3, pp. 45–55, 1980, doi: 10.1016/0378-1127(80)90004-3.

- [30] N. Das, S. K. Mishra, A. Bishayee, E. S. Ali and A. Bishayee, "The phytochemical, biological, and medicinal attributes of phytoecdysteroids: An updated review," *Acta Pharm. Sin. B.*, vol. 11, no. 7, pp. 1740–1766, Jul. 2021, doi: 10.1016/j.apsb.2020.10.012.
- [31] S. Adjei *et al.*, "Fruits of *Vitex doniana* sweet: toxicity profile, anti-inflammatory and antioxidant activities, and quantification of one of its bioactive constituents oleanolic acid," *Heliyon*, vol. 7, no. 9, p. e07910, Sept. 2021, doi: 10.1016/j.heliyon.2021.e07910.
- [32] J. P. Sawant, S. F. Shaikh, R. B. Kale and H. M. Pathan, "Chemical Bath Deposition of CulnS₂ Thin Films and Synthesis of CulnS₂ Nanocrystals: A Review," *Eng. Sci.*, vol. 12, pp. 1–12, Jan. 2020, doi: 10.30919/es8d1142.
- [33] A. A. Bunaciu, E. G. Udriștioiu and H. Y. Aboul-Enein, "X-Ray Diffraction: Instrumentation and Applications," *Crit. Rev. Anal. Chem.*, vol. 45, no. 4, pp. 289–299, May 2015, doi: 10.1080/10408347.2014.949616.
- [34] N. K. Elumalai, C. Vijila, R. Jose, A. Uddin and S. Ramakrishna, "Metal oxide semiconducting interfacial layers for photovoltaic and photocatalytic applications," *Mater. Renew. Sustain. Energy*, vol. 4, no. 11, 2015, doi: 10.1007/s40243-015-0054-9.
- [35] S. Fan, L. Li, X. Wang, C. Gua and J. Tu, "Metal oxide/hydroxide-based materials for supercapacitors," *RSC Adv.*, vol. 79, pp. 41910–41921, 2014, doi: 10.1039/C4RA06136E.
- [36] L. Fang *et al.*, "Fabrication of hybrid cauliflower-like nanoarchitectures by in situ grown ZnO nanoparticals on VS₂ ultrathin nanosheets for high performance supercapacitors," *Colloids Surf. A Physicochem. Eng. Asp.*, vol. 501, pp. 42–48, Jul. 2016, doi: 10.1016/j.colsurfa.2016.04.047.
- [37] P. Prabakaran, S. Prabhu, M. Selvaraj, M. Navaneethan, P. Ramu and R. Ramesh, "Synthesis of r-GO-incorporated CoWO₄ nanostructure for high-performance supercapattery applications," *J. Mater. Sci. Mater. Electron.*, vol. 33, pp. 9312–9323, Nov. 2021, doi: 10.1007/s10854-021-07297-0.
- [38] S. H. Kim, Y. I. Kim, J. H. Park and J. M. Ko, "Cobalt-Manganese Oxide/Carbon-Nanofibre Composite Electrodes for Supercapacitors," *Int. J. Electrochem. Sci.*, vol. 4, no. 11, pp. 1489–1496, Nov. 2009, doi: 10.1016/S1452-3981(23)15239-4.
- [39] S. W. Kim *et al.*, "Electrochemical performance and ex situ analysis of ZnMn₂O₄ nanowires as anode materials for lithium rechargeable batteries," *Nano Res.*, vol. 4, pp. 505–510, Feb. 2011, doi: 10.1007/s12274-011-0106-0.
- [40] N. Priyadharsini, A. Shanmugavani, L. Vasylechko and R. K. Selvan, "Sol-gel synthesis, structural refinement, and electrochemical properties of potassium manganese phosphate for supercapacitors," *Ionics*, vol. 24, no. 7, pp. 2073–2082, Jan. 2018, doi: 10.1007/s11581-018-2449-y.

- [41] M. Al-Omair, A. Touny and M. Saleh, "Reflux-based synthesis and electrocatalytic characteristics of nickel phosphate nanoparticles," *J. Power Sources*, vol. 342, pp. 1032–1039, Feb. 2017, doi: 10.1016/j.jpowsour.2016.09.079.
- [42] N. N. Prokopchuk, V. A. Kopilevich and L. V. Voitenko, "Preparation of double nickel(II) cobalt(II) phosphates with controlled cationic composition," *Russ. J. Appl. Chem.*, vol. 81, no. 3, pp. 386–391, May 2008, doi: 10.1134/S1070427208030063.
- [43] D. Yang, Q. Yu, L. Gao, L. Mao and J. Yang, "The additive effect of graphene in nickel phosphate/graphene composite and enhanced activity for electrochemical oxidation of methanol," *Appl. Surf. Sci.*, vol. 416, pp. 503–510, Sept. 2017, doi: 10.1016/j.apsusc.2017.04.208.
- [44] P. Noisong, C. Danvirutai, T. Srithanratana and B. Boonchom, "Synthesis, characterization and non-isothermal decomposition kinetics of manganese hypophosphite monohydrate," *Solid State Sci.*, vol. 10, no. 11, pp. 1598–1604, Nov. 2008, doi: 10.1016/j.solidstatesciences.2008.02.020.
- [45] T. P. Vijitha and D. Saranya, "Corn Silk A Medicinal Boon," *Int. J. ChemTech Res.*, vol. 10, no. 10, pp. 129–137, 2017.
- [46] M. Zhang *et al.*, "Study of pseudocapacitive contribution to superior energy storage of 3D heterostructure CoWO₄/Co₃O₄ nanocone arrays," *J. Power Sources*, vol. 418, pp. 202–210, Apr. 2019, doi: 10.1016/j.jpowsour.2019.02.041.
- [47] M. M. Faisal, S. R. Ali, M. Z. Iqbal, M. W. Iqbal, A. Numan and K. Sanal, "Effect of polyaniline on the performance of zinc phosphate as a battery-grade material for supercapattery," *J. Energy Storage*, vol. 44, p. 103329, Dec. 2021, doi: 10.1016/j.est.2021.103329.
- [48] N. S. Punde, A. S. Rajpurohit and A. K. Srivastava, "Fabrication of an Advanced Symmetric Supercapattery Based on Nanostructured Bismuth-Cobalt-Zinc Ternary Oxide Anchored on Silicon Carbide Hybrid Composite Electrode," *Energy Technol.*, vol. 7, no. 9, p. 1900387, Sept. 2019, doi: 10.1002/ente.201900387.
- [49] G. He *et al.*, "Dumbbell-like ZnO nanoparticles-CeO₂ nanorods composite by one-pot hydrothermal route and their electrochemical charge storage," *Appl. Surf. Sci.*, vol. 366, pp. 129–138, Mar. 2016, doi: 10.1016/j.apsusc.2016.01.027.
- [50] A. Arshad, J. Iqbal and Q. Mansoor, "NiO-nanoflakes grafted graphene: an excellent photocatalyst and a novel nanomaterial for achieving complete pathogen control," *Nanoscale*, vol. 42, pp. 16321–16328, 2017, doi: 10.1039/C7NR05756C.
- [51] A. K. Das, U. S. V. Pan, N. H. Kim and J. H. Lee, "Nanostructured CeO₂/NiV-LDH composite for energy storage in asymmetric supercapacitor and as methanol oxidation electrocatalyst," *Chem. Eng. J.*, vol. 417, p. 128019, Aug. 2021, doi: 10.1016/j.cej.2020.128019.

- [52] R. M. Obodo *et al.*, "Evaluation of 8.0 MeV Carbon (C²⁺) Irradiation Effects on Hydrothermally Synthesized Co₃O₄-CuO-ZnO@GO Electrodes for Supercapacitor Applications," *Electroanalysis*, vol. 32, no. 12, pp. 2958–2968, Dec. 2020, doi: 10.1002/elan.202060382.
- [53] M. M. Faisal, S. R. Ali, M. Z. Iqbal, M. Z. Iqbal, M. W. Iqbal, A. Numan and K. C. Sanal, "Effect of polyaniline on the performance of zinc phosphate as a battery-grade material for supercapattery," *J. Energy Storage*, vol. 44, p. 103329, Dec. 2021, doi: 10.1016/j.est.2021.103329.
- [54] R. K. Muhammad *et al.*, "Cerium oxide nanosheets-based tertiary composites (CeO₂/ZnO/ZnWO₄) for supercapattery application and evaluation of faradic & nonfaradic capacitive distribution by using Donn's model," *J. Energy Storage*, vol. 55, p. 105778, Nov. 2022, doi: 10.1016/j.est.2022.105778.
- [55] G. G. Amatucci, F. Badway, A. Du Pasquier and T. Zheng, "An Asymmetric Hybrid Nonaqueous Energy Storage Cell," *J. Electrochem. Soc.*, vol. 148, p. A930, Jul. 2001, doi: 10.1149/1.1383553.
- [56] R. M. Obodo *et al.*, "Annealing optimization of graphitized Co₃O₄@CuO@NiO composite electrodes for supercapacitor applications," *Energy Storage*, vol. 4, no. 5, p. e347, Oct. 2022, doi: 10.1002/est2.347.
- [57] S. J. Marje *et al.*, "Microsheets like nickel cobalt phosphate thin films as cathode for hybrid asymmetric solid-state supercapacitor: Influence of nickel and cobalt ratio variation," *Chem. Eng. J.*, vol. 429, p. 132184, Feb. 2022, doi: 10.1016/j.cej.2021.132184.
- [58] Y. M. Chen, J. H. Cai, Y. S. Huang, K. Y. Lee and D. S. Tsai, "Preparation and characterization of iridium dioxide—carbon nanotube nanocomposites for supercapacitors," *Nanotechnology*, vol. 22, p. 115706, Feb. 2011, doi: 10.1088/0957-4484/22/11/115706.
- [59] A. C. Nkele *et al.*, "Recent Advances in Materials for Supercapacitors," *Nano-Horizons*, vol. 1, no. 1, pp. 1–32, Sept. 2022, doi: 10.25159/NanoHorizons.53db1f5bd625.
- [60] W. Li, Y. Bu, H. Jin, J. Z. J. Wang, S. Wang and J. Wang, "The Preparation of Hierarchical Flowerlike NiO/Reduced Graphene Oxide Composites for High Performance Supercapacitor Applications," *Energy Fuels*, vol. 27, no. 10, pp. 6304–6310, Sept. 2013, doi: 10.1021/ef401190b.
- [61] Y. Zhang, Y. Zhang, Y. Zhang, H. Si and L. Sun, "Bimetallic NiCo₂S₄ Nanoneedles Anchored on Mesocarbon Microbeads as Advanced Electrodes for Asymmetric Supercapacitors," *Nano-Micro Lett.*, vol. 11, p. 11, Apr. 2019, doi: 10.1007/s40820-019-0265-1.

Obodo et al.

- [62] R. M. Obodo *et al.*, "Fabrication of Co₃(PO₄)₂@Mn₃(PO₄)₂@Ni₃(PO₄)₂ electrodes optimized using *Vitex doniana* leaf extract for supercapacitor application," *Ionics*, vol. 30, pp. 4951–4965, Jun. 2024, doi: 10.1007/s11581-024-05631-0.
- [63] R. M. Obodo *et al.*, "Enhancement of synergistic effects of Cu₂O@MnO₂@NiO Using *Sarcophrynium Brachystachys* leaf extract for supercapacitor electrode application," *Next Mater.*, vol. 5, p. 100244, Oct. 2024, doi: 10.1016/j.nxmate.2024.100244.
- [64] R. M. Obodo *et al.*, "Optimization of MnO₂, NiO and MnO₂@NiO electrodes using graphene oxide for supercapacitor applications," *Curr. Res. Green Sustain. Chem.*, vol. 5, p. 100345, 2022, doi: 10.1016/j.crgsc.2022.100345.